

We are IntechOpen, the world's leading publisher of Open Access books Built by scientists, for scientists

6,900

Open access books available

185,000

International authors and editors

200M

Downloads

Our authors are among the

154

Countries delivered to

TOP 1%

most cited scientists

12.2%

Contributors from top 500 universities



WEB OF SCIENCE™

Selection of our books indexed in the Book Citation Index
in Web of Science™ Core Collection (BKCI)

Interested in publishing with us?
Contact book.department@intechopen.com

Numbers displayed above are based on latest data collected.
For more information visit www.intechopen.com



Study and Design of Reconfigurable Wireless and Radio-Frequency Components Based on RF MEMS for Low-Power Applications

Bassem Jmai, Adnen Rajhi, Paulo Mendes and Ali Gharsallah

Additional information is available at the end of the chapter

<http://dx.doi.org/10.5772/intechopen.74785>

Abstract

This chapter intends to deal with the challenging field of communication systems known as reconfigurable radio-frequency systems. Mainly, it will present and analyze the design of different reconfigurable components based on radio-frequency microelectromechanical systems (RF MEMS) for different applications. This chapter will start with the description of the attractive properties that RF MEMS structures offer, giving flexibility in the RF systems design, and how these properties may be used for the design of reconfigurable RF MEMS-based devices. Then, the chapter will discuss the design, modeling, and simulation of reconfigurable components based on both theoretical modeling and well-known electromagnetic computing tools such as ADS, CST-MWS, and HFSS to evaluate the performance of such devices. Finally, the chapter will deal with the design and performance assessment of RF MEMS-based devices. Non-radiating devices, such as phase shifter and resonators, which are very important components in the hardware RF boards, will be addressed. Also, three types of frequency reconfigurable antennas, for the three different applications (radar, satellite, and wireless communication), will be proposed and evaluated. From this study, based on theoretical design and electromagnetic computing evaluation, it has been shown that RF MEMS-based devices can be an enabling solution in the design of the multiband reconfigurable radio-frequency devices.

Keywords: RF MEMS capacitive switch, modeling, tunable, MMIC, phase shifter, RF resonator, frequency reconfigurable antennas

1. Introduction

The extraordinary evolution and the knowledge built-in the radio-frequency field were noticed in various applications such as militaries, medicine, and telecommunication. At the system level, one trend in the field of wireless telecommunications is the design of multiband and multimode devices, with an ever-increasing number of features, leading to the so pursued reconfigurable systems.

At present, reconfigurable systems have become very promising in a wide range of applications, including future services of wireless communication systems. However, the wide spread of wireless communication systems and the emergence of new wireless communication standards have introduced new challenges in the hardware design for transmitters and receivers. To tackle this problem, nowadays telecommunication systems need to use a significant number of tunable components, where the performance is degraded when compared to their equivalents at fixed frequencies.

A telecommunication system is said to be tunable or reconfigurable, when some of its characteristics (central frequency, bandwidth, polarization, etc.) can be modified by an external control signal (electrical, mechanical, thermal, etc.). Despite tunable components can be realized using many different designs, mainly, two approaches exist for tunability:

- The first way is achieved by the possibility to change the substrate permittivity (ferroelectric [1] and ferromagnetic [2]).
- The second way consists in a change of the capacitive or the inductive load by the addition of tunable radio-frequency integrated circuits (RFIC). This method relies on semiconductor devices (diode [3] and transistors [4]) or mechanical (RF MEMS [5]) components.

The RF MEMS devices feature low-power consumption, high linearity, wide bandwidth, and high dynamic range, which are among the most important requirements that each component must meet in order to achieve high-performance wireless systems.

This chapter will present the development of frequency and phase reconfigurable components, based on capacitive tunable RF MEMS.

2. RF MEMS technologies

RF MEMS has its origin in the MEMS systems, which are miniature electronic and/or mechanical systems designed to perform specific tasks. They consist of motors, gears, levers, electrical devices, or tiny sensors. These devices are used in many applications and their size range from a few micrometers to a few millimeters. By the late 1960s, MEMS systems were used as precise sensors of hydraulic pressure in aircraft. Today, these systems play an important and ever-increasing role in the fields of medicine (detection of organic cells), automotive (accelerometer

in airbag triggering), entertainment (motion detection in a video game), and optics (micro mirrors), to mention just a few applications.

2.1. What is RF MEMS?

MEMS devices have found application in many different fields. As shown in **Figure 1**, the MEMS components can be classified into four main families [6]:

- **Sensors:** miniaturized systems, made from microtechnologies used for sensor applications in measurement and instrumentation fields, such as pressure sensors and capacitive accelerometer.
- **MOEMS:** this type of MEMS can be used in optical technologies, such as micro mirrors, optical switches, and optical cavities.
- **Bio-MEMS:** miniaturized systems, made from micro- and nanotechnologies derived from microelectronics (integrated circuits) which is intended to carry out experiments in biology/chemistry, such as DNA chip, microchemical reactor, and micro valves.
- **RF MEMS:** in the field of microwaves, they improve the performance of tunable devices to various functions, such as variable passive components, resonators, filters, and antennas.

In this way, RF MEMS is usually related with the application of MEMS technologies to develop systems that contribute to the RF system development. They can be used to increase the performance or to implement characteristics not achievable by other solutions, even if performance is slightly degraded. Despite a few drawbacks, the emergence of RF MEMS represents a revolution in the development of new radio-frequency systems. In fact, these elements should compete or replace certain semiconductor components in microwave applications. They are very compact (typically a few hundred square micrometers) and can be up to 50% smaller than semiconductor components performing the same function [7].

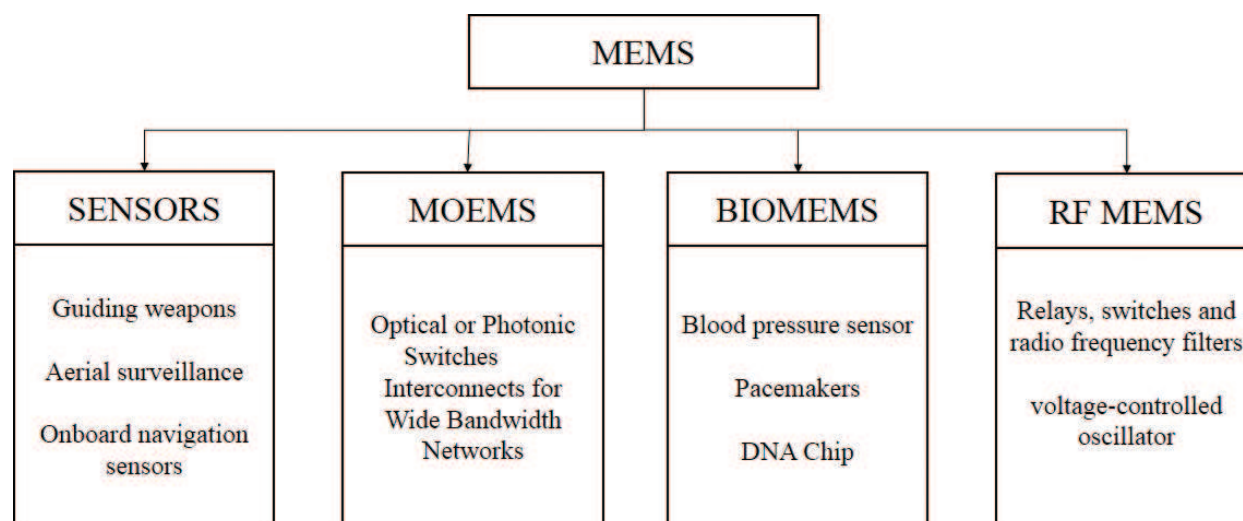


Figure 1. MEMS families.

2.2. RF MEMS switch as a building block

The microelectromechanical components enable the reconfiguration of electronic devices using mechanical movements. Using this feature, one building block widely used to enable a device’s tunability is the MEMS switch, and we call it a MEMS microswitch. The microelectromechanical part of the microswitch, or varactor components, has the form of a mobile beam suspended and anchored to one of its ends. The beam can be built-in, or double-embedded. The main idea behind a tunable device is the fact that when a MEMS switch moves, besides switching from on and off states, it may exhibit a different RF load. And controlling such RF load, it is possible to tune different RF devices.

2.3. RF MEMS switch control mechanism

The mechanical movement of the beam is obtained by applying an actuating force. This actuating force is generally of an electrostatic nature [8, 9], but it can be thermal [10], piezoelectric [11], or magnetic [12]. **Table 1** is showing the comparative study of the different types of actuation [8, 13].

Electrostatic actuators are the most used components because they consume very little, occupy a very small volume, and has a short switching time. In this chapter, the electrostatically actuated RF MEMS will be explored as a solution for different applications.

2.4. RF MEMS switches topologies

RF MEMS microswitches are components intended to perform an electrical function through the control of a movable or mechanically deformable structure. There are two main types of RF MEMS components: the capacitive touch switch (contact: metal-dielectric-metal) and the resistive or ohmic contact switch (contact: metal-metal). In both cases, it is necessary to apply a force to the movable part of the component to move the MEMS beam. In this work, we will only be interested in RF MEMS capacitive shunt switch based on electrostatic actuators.

In order to summarize the previous points for RF MEMS, **Table 2** makes a comparison between the two types, ohmic and capacitive, and their configurations [14–17].

Type of switching	Switching speed (μs)	Switch size	Consumption (mW)
Electrostatic	0.05–200	Small	~0
Thermal	50–200	Medium	<100
Piezoelectric	1–200	Medium	~0
Magnetic	500–4000	Large	<200

Table 1. Comparison of the different types of actuation.

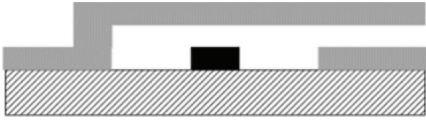



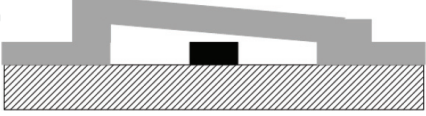
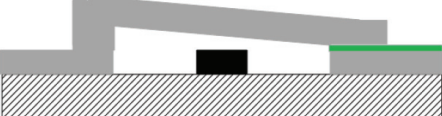


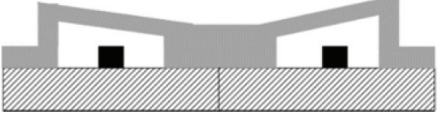
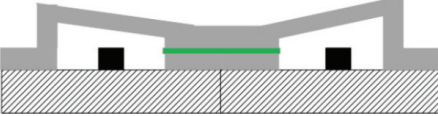
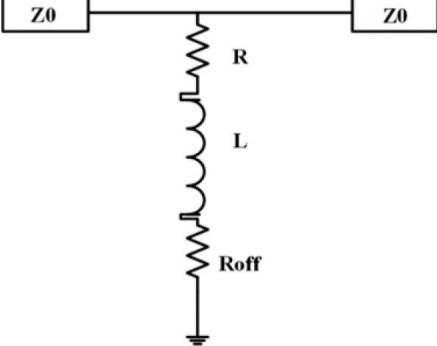
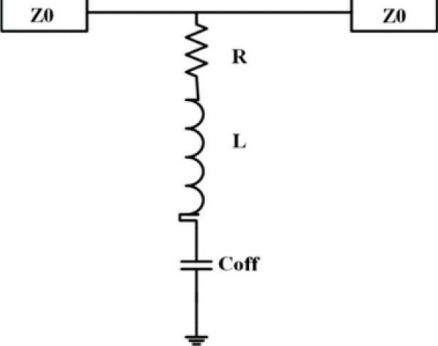
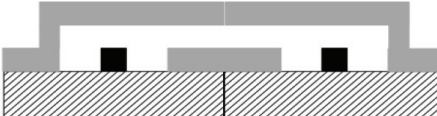
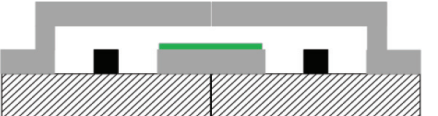
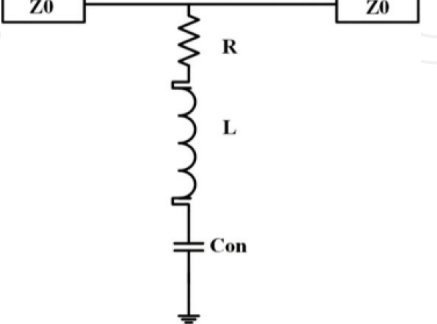
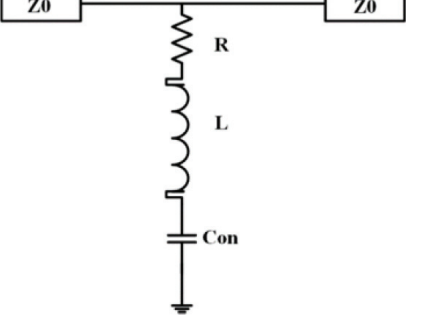
		Ohmic	Capacitive
Cantilever	OFF		
		<div>R L C_{off}</div> 	<div>R L C_{off}</div> 
	ON		
		<div>R L R_{on}</div> 	<div>R L C_{on}</div> 
Fixed-fixed beam	OFF		
		<div>Z0 R L R_{off}</div> 	<div>Z0 R L C_{off}</div> 
	ON		
		<div>Z0 R L C_{on}</div> 	<div>Z0 R L C_{on}</div> 

Table 2. Classification of RF MEMS switches: cantilever and fixed beam, capacitive and ohmic, series, and shunt electrical model of MEMS switches.

3. Capacitive RF MEMS mechanical modeling

Before designing any device using RF MEMS technology, it is required to understand the behavior of the main block, the switch. In this way, the first design step will be to compute the applied force a moving beam suffers due to an external electric field. It will be derived considering that the control signal is an electric potential applied between the movable beam and an activation electrode.

3.1. Capacitive RF MEMS device configuration

The performance, as well the analysis used to improve the RF MEMS device, is heavily dependent on the study of the bridge. **Figure 2** presents the proposed RF MEMS switch, with small dimensions ($1200 \times 900 \times 681 \mu\text{m}^3$). This RF MEMS is based on CPW technology ($G/S/G = (90/120/90)$).

This RF MEMS varactor structure has a multilayer configuration. The used substrate is based on silicon (Si) with thickness of $675 \mu\text{m}$. The second layer is made of a silicon dioxide (SiO_2) with thickness equal to $2 \mu\text{m}$ and a CPW line circuit metal based on copper with thickness of $1 \mu\text{m}$. The bridge has a depth of $1 \mu\text{m}$, with ends attached to the groundline of the CPW by an epoxy (polymer based on negative-tone photoresist SU-8 2000.5 with $3 \mu\text{m}$ thickness). The dielectric is fabricated through a silicon nitride (Si_3N_4) with depth equal to $1 \mu\text{m}$.

3.2. Mechanical model

The first step when modeling a RF MEMS device is to determine the electromechanical behavior of the switch, meaning that we want to understand how, and how much, the structure will move in response to an applied voltage.

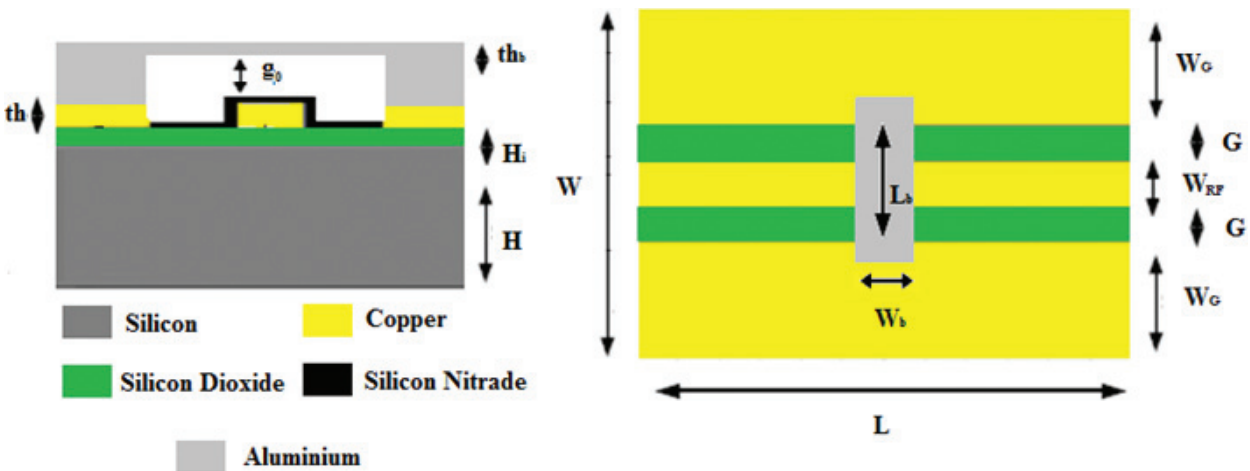


Figure 2. Design of the proposed capacitive RF MEMS device.

The uniform bridge of MEMS is geometrically simple since it is only a rectangular suspension located above a tape connected to contact pads by the sides of the same width, as shown in **Figure 3** [18].

Nominal capacity: the capacitance C between the two electrodes is given by:

The mechanical model of deformable flat capacity is given by Eq. (1), where g is the height between the low beam and the electrode. The bridge width is denoted by W_b and the length of the ground electrode by W :

$$C = \epsilon_0 \frac{W_b W}{g} \quad (1)$$

The height depends on the voltage applied between the electrodes. In the absence of voltage ($V = 0$), the height is equal to g_0 and the capacity is named C_0 [8]:

$$dW_t = dW_e - dW_m = (V.dq) - (F_e.dg_e) \quad (2)$$

where q is the quantity of charge accumulated in the capacity and F_e is the electrostatic force.

The well-known equation of potential of electrostatic energy is given by Eq. (3):

$$U_E(j) = \frac{1}{2} C(V).V^2 \quad (3)$$

Then, the electrostatic force for a flat capacity can be expressed by Eq. (4):

$$F_e = \frac{\partial W_e}{\partial g} = -\frac{1}{2} \epsilon_0 \frac{W_b W}{g^2} V^2 \quad (4)$$

The mechanical behavior of the beam can be modeled by a spring of constant k_z . This induces a mechanical force (F_m) exerted by the bridge. This force is the opposite of F_e and it is defined by Eq. (5):

$$F_m = -F_e = k_z (g_0 - g) = -\frac{1}{2} \epsilon_0 \frac{W_b W}{g^2} V^2 \quad (5)$$

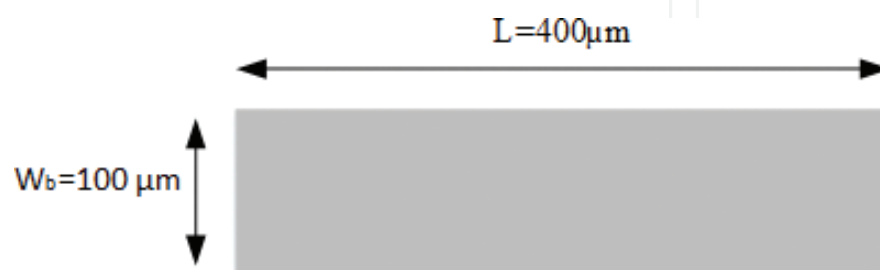


Figure 3. The beam of the MEMS under analysis.

From this equation, we can then conclude a relationship between the height of the air gap g and the applied voltage V :

$$0 = g^3 - g_0 g^2 + \frac{1}{2k_m} \varepsilon_0 W_b W V^2 \quad (6)$$

The relationship between the applied voltage and the spacing g parameter is given in Eq. (7):

$$V_p = \sqrt{\frac{2k_z}{\varepsilon_0 W_b W} g^2 (g_0 - g)} \quad (7)$$

$$k_z = \frac{1}{2} \left(32 E w \left(\frac{t}{l} \right)^3 + 8 \sigma (1 - \nu) w \left(\frac{t}{l} \right) \right). \quad (8)$$

where E is the Young's modulus, σ is the residual stress of the beam, ν is the Poisson's coefficient, t is the thickness, and l is the length of the bridge.

In **Table 3**, the mechanical properties (Young's modulus, Poisson's ratio, residual stress, and density) of four different bridge materials (nickel, copper, aluminum, and gold) are presented.

In terms of control voltage, comparatively the nickel presents a bad choice, since the required voltage to obtain some deflection is near twice the voltage that is required for gold and aluminum. However, the gold price presents an obstruction, being the best choice, in this comparative study, the aluminum.

The bridge was simulated using COMSOL multiphysic and reaches a deflection equal to $2 \mu\text{m}$. The obtained simulation results are given in **Figure 4** for applied voltage equal to 25 V. The relationship between the capacitance and the applying voltage is shown in **Figure 5**.

3.3. RF MEMS switch design parameters

We will present next the relevant parameters that define the variable MEMS capacity.

Tuning range: the "tuning range" or variation of the capacity is an important factor of the variance MEMS capacities. It is defined as

Material	Nickel	Copper	Aluminum	Gold
Young's modulus E (GPa)	200	120	69	79
Poisson's ratio	0.31	0.355	0.345	0.42
Residual stress σ (MPa)	20	20	20	20
Density (kg/m^3)	8900	8960	2700	19,300
Pull-down voltage simulated result [V]	46	34	25	22

Table 3. Mechanical parameters of different materials of the bridge.

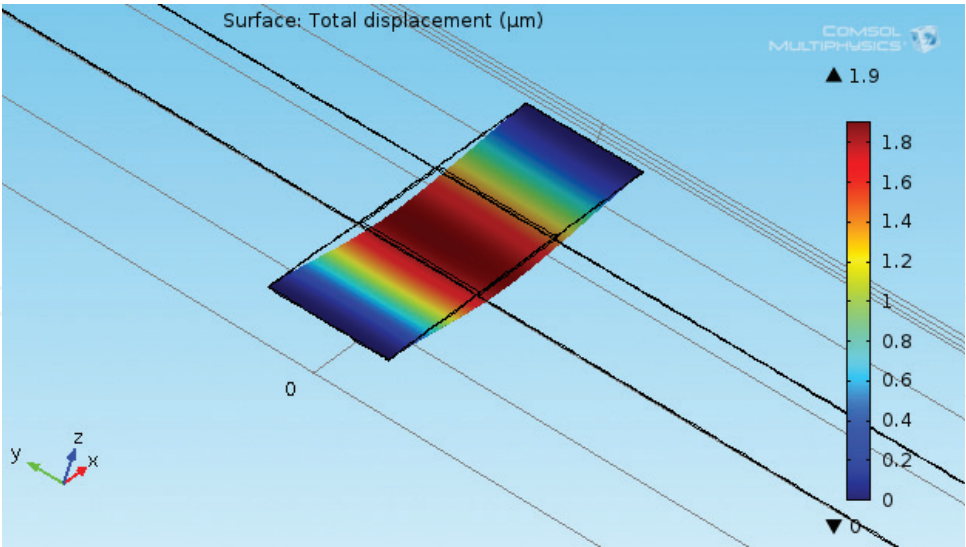


Figure 4. Simulation results of the beam.

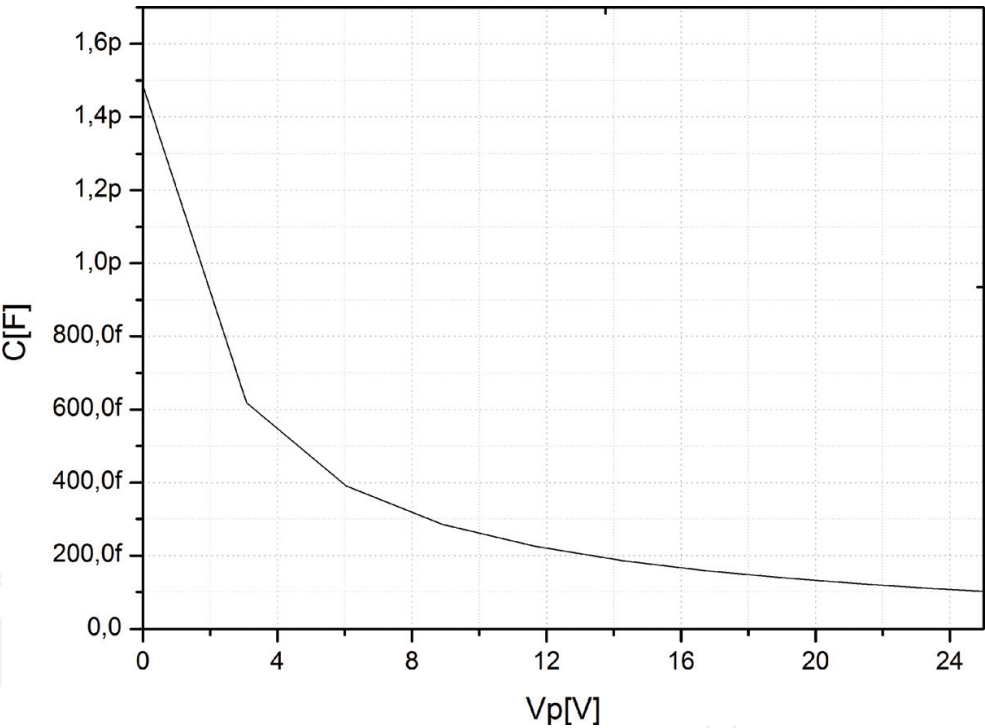


Figure 5. Relationship between the capacity and the voltage applied.

$$TR = \frac{C_{\max} - C_{\min}}{C_{\min}} \tag{9}$$

Quality factor: the quality factor Q of a component is an important parameter. Indeed, it determines the losses of a variable filter or the noise of a VCO using a variable capacity. It is defined by the ratio between the energy stored and the energy lost by the component:

$$Q = \frac{\text{Lost energy per cycle}}{\text{Total energy per cycle}} \tag{10}$$

Linearity: the nonlinearity of the passive components is an important and demanding data for radio-frequency applications. In fact, we want to obtain the value of the linear capacity as a function of the frequency and the actuating voltage.

4. Capacitive RF MEMS electrical modeling

Once the mechanical response to the control voltage is known, the next step will be to model the RF load that the switch will present to a transmission line. That load will be the variable that can be controlled to obtain RF tunable devices or systems.

4.1. RF modeling approach

Figure 6 shows the proposed model of the proposed RF MEMS [19]. The proposed circuit model consists of two CPW lines, separated by a shunt RLC circuit. The RLC is the equivalent bridge circuit.

The MEMS can be modeled by the association of three subsystems in cascade. The ABCD matrix is given by Eq. (11):

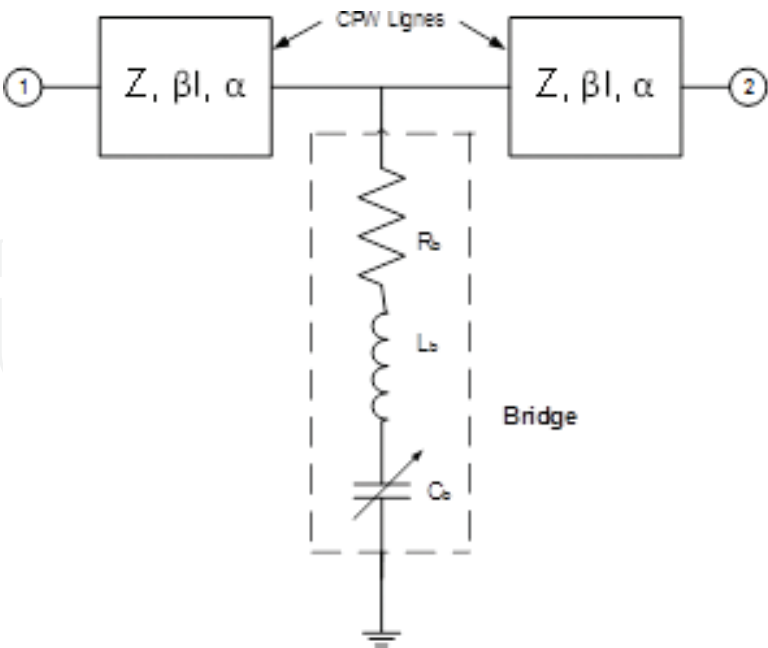


Figure 6. Electromagnetics model.

$$\begin{bmatrix} A & B \\ C & D \end{bmatrix} = \underbrace{\begin{bmatrix} A_1 & B_1 \\ C_1 & D_1 \end{bmatrix}}_{TL1} * \underbrace{\begin{bmatrix} A_b & B_b \\ C_b & D_b \end{bmatrix}}_{Bridge} * \underbrace{\begin{bmatrix} A_2 & B_2 \\ C_2 & D_2 \end{bmatrix}}_{TL2} \quad (11)$$

Considering a system represented by an association of three devices where the ABCD matrix is known, the next step is to determine each subsystem matrix.

4.1.1. Coplanar waveguide modeling

The CPW's most important electrical parameters are the characteristic impedance Z_C and the effective permittivity ϵ_{eff} , both given by Eq. (12), where $K(k)$ and $K'(k)$ present the elliptic integral which essentially depends on the CPW's geometric and physical characteristics. Here, ϵ_r is the relative permittivity, w is the width of the RF line, s is the gap between the RF line and ground, h is the thickness of substrate, and h_1 is the thickness of the buffer layer:

$$\begin{cases} Z_C = \frac{30\pi}{\sqrt{\epsilon_{eff}}} \frac{K'(k)}{K(k)} \\ \epsilon_{eff} = 1 + \frac{\epsilon_r - 1}{2} \frac{K'(k)K(k_1)}{K(k)K'(k_1)} \end{cases} \quad (12)$$

$$\begin{cases} k = \frac{w}{w + 2s} \\ k_1 = \frac{sh\left(\frac{\pi w}{4h}\right)}{sh\left(\frac{\pi(w + 2s)}{2h}\right)} \end{cases} \quad (13)$$

$$\begin{cases} K'(k) = K(k') \\ k' = \sqrt{1 - k^2} \end{cases} \quad (14)$$

The ratio $K(k)/K'(k)$ approximation is done by Eq. (15):

$$\frac{K(k)}{K'(k)} = \begin{cases} 0 \leq k \leq \frac{1}{\sqrt{2}} \Rightarrow \frac{K(k)}{K'(k)} = \frac{\pi}{\ln\left(2 \frac{1 + \sqrt{k}}{1 - \sqrt{k}}\right)} \\ \frac{1}{\sqrt{2}} \leq k \leq 1 \Rightarrow \frac{K(k)}{K'(k)} = \frac{1}{\pi} \ln\left(2 \frac{1 + \sqrt{k}}{1 - \sqrt{k}}\right) \end{cases} \quad (15)$$

The second parameter for modeling the CPW line is the propagation constant. This parameter is given by Eq. (16), as a function of the attenuation constant and the phase constant. The attenuation constant is due to the conductor as well as to the attenuation in dielectric, both presented in Eq. (17):

$$\gamma = \alpha + j\beta \begin{cases} \alpha = \alpha_c + \alpha_d \\ \beta = \frac{2\pi}{\lambda}; \lambda = \frac{c}{f\sqrt{\epsilon_{eff}\mu_{eff}}}; c = 3 \times 10^8 \text{ m s}^{-1} \end{cases} \quad (16)$$

$$\begin{cases} \alpha_d = 27.3 \frac{\epsilon_r}{\epsilon_r - 1} \frac{\epsilon_{eff}(f) - 1}{\sqrt{\epsilon_{eff}(f)}} \frac{\tan\delta}{\lambda_0} \text{ (dB/lenght)} \\ \alpha_c = \frac{8.68R_s}{480\pi K(k_1)K(k'_1)(1 - k_1^2)} \left[\frac{1}{a} \left(\pi + \text{Ln} \left(\frac{8a\pi(1 - k_1)}{t(1 + k_1)} \right) \right) + \frac{1}{b} \left(\pi + \text{Ln} \left(\frac{8b\pi(1 - k_1)}{t(1 + k_1)} \right) \right) \right] \text{ (dB/lenght)} \end{cases} \quad (17)$$

The model of CPW line is presented by ABCD matrix in Eq. (18):

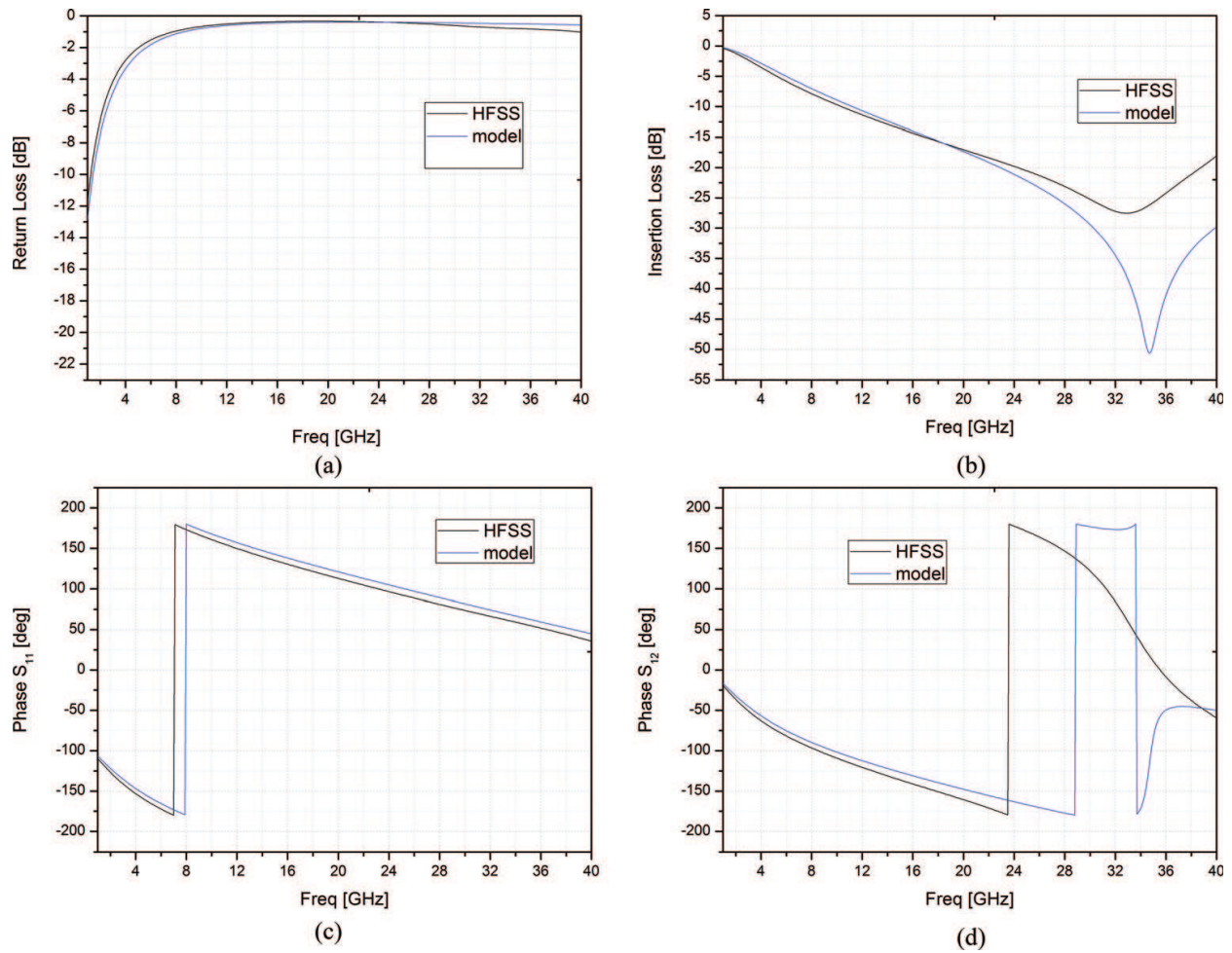


Figure 7. Simulation results of the scattering parameters versus frequency at the OFF state: (a) return loss, (b) insertion loss, (c) phase of S_{11} , (d) phase of S_{12} .

$$\begin{bmatrix} A & B \\ C & D \end{bmatrix} = \begin{bmatrix} \cosh(\gamma L) & Z_c \sinh(\gamma L) \\ \frac{\sinh(\gamma L)}{Z_c} & \cosh(\gamma L) \end{bmatrix} \quad (18)$$

4.1.2. Bridge modeling

The bridge is modeled by an inductor (L_b) and a resistance (R_b) in series. These parameters are independent of the substrate. The proposed RF MEMS has a capacitive variable (C_b). The parameters (L_b), (R_b), and (C_b) are given by Eqs. (19) and (20):

$$\begin{cases} R_b = \frac{L}{\sigma w t} \\ L_b = 0.2 * [(\ln(L/(w + t))) + 1.193 + 0.2235 * ((w + t)/L)] * L \end{cases} \quad (19)$$

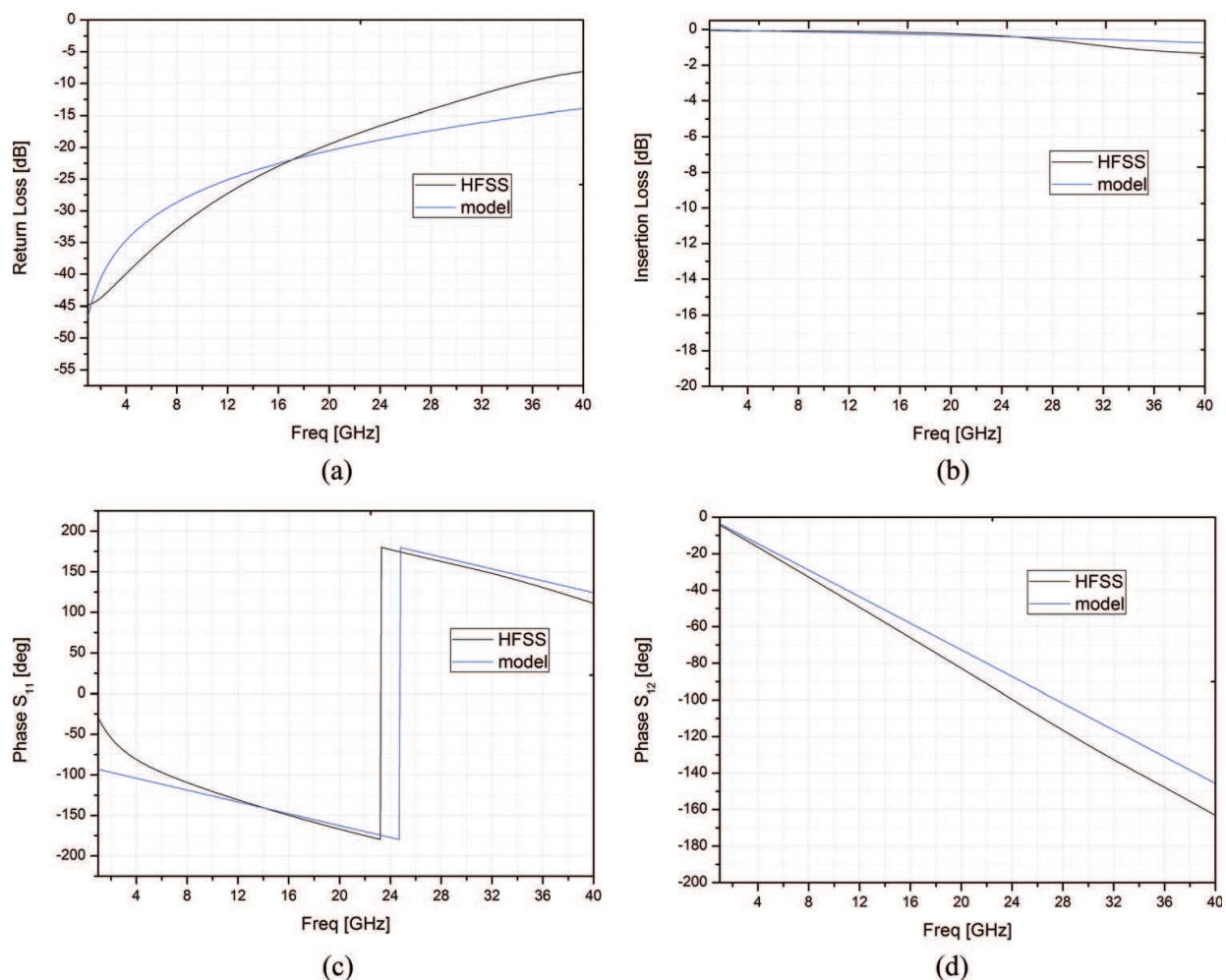


Figure 8. Simulation results of the scattering parameters versus frequency at the ON state: (a) return loss, (b) insertion loss, (c) phase of S_{11} , (d) phase of S_{12} .

$$c_b = \begin{cases} c_{down} = \frac{\epsilon_0 \epsilon_r A}{th} \\ c_{up} = \frac{\epsilon_0 A}{g_0 + \frac{th}{\epsilon_r}} \end{cases} \quad (20)$$

The bridge model can be presented by the next ABCD matrix:

$$\begin{bmatrix} A_b & B_b \\ C_b & D_b \end{bmatrix} = \begin{bmatrix} 1 & 0 \\ \frac{1}{Z_b} & 1 \end{bmatrix} = \begin{bmatrix} 1 & 0 \\ \frac{1}{R_b + jX_b} & 1 \end{bmatrix} = \begin{bmatrix} 1 & 0 \\ \frac{1}{R_b + j(L_b\omega + 1/C_b\omega)} & 1 \end{bmatrix} \quad (21)$$

4.2. The scattering parameters model

The standard output of simulation tools is the S-parameters. In this way, we need to transform the previous developed model to present it in a convenient way to allow comparison with such tools. The scattering parameters can be expressed by the following form:

$$\begin{bmatrix} S_{11} & S_{12} \\ S_{21} & S_{22} \end{bmatrix} = \begin{bmatrix} \frac{A + B/Z_0 - CZ_0 - D}{A + B/Z_0 + CZ_0 + D} & \frac{2(AD - BC)}{A + B/Z_0 + CZ_0 + D} \\ \frac{2}{A + B/Z_0 + CZ_0 + D} & \frac{-A + B/Z_0 - CZ_0 + D}{A + B/Z_0 + CZ_0 + D} \end{bmatrix} \quad (22)$$

where the reflection coefficient and its phase are given by Eq. (23) and the insertion loss and its phase are given by Eq. (24). The scattering parameters are written in the following form:

$$S_{11} = S_{22} = |S_{11}|e^{j\Phi_{11}} = \frac{(Z_c^2 - Z_0^2) + 2R_bZ_c + j2Z_cX_b}{((Z_0 + Z_c)^2 + 2R_b(Z_0 + Z_c)) + j2X_b(Z_0 + Z_c)}$$

$$\Rightarrow \begin{cases} |S_{11}| = \left\{ \frac{\sqrt{((Z_c^2 - Z_0^2) + 2R_bZ_c)^2 + (2Z_cX_b)^2}}{\sqrt{((Z_0 + Z_c)^2 + 2R_b(Z_0 + Z_c))^2 + (2X_b(Z_0 + Z_c))^2}} \right\} \\ \Phi_{12} = tg^{-1}\left(\frac{2Z_cX_b}{2R_bZ_c}\right) - tg^{-1}\left(\frac{2X_b(Z_0 + Z_c)}{((Z_0 + Z_c)^2 + 2R_b(Z_0 + Z_c))}\right) \end{cases} \quad (23)$$

$$S_{12} = S_{21} = |S_{12}|e^{j\Phi_{12}} = \frac{2R_bZ_c + j2Z_cX_b}{((Z_0 + Z_c)^2 + 2R_b(Z_0 + Z_c)) + j2X_b(Z_0 + Z_c)}$$

$$\Rightarrow \begin{cases} |S_{12}| = \frac{\sqrt{(2R_bZ_c)^2 + (2Z_cX_b)^2}}{\sqrt{((Z_0 + Z_c)^2 + 2R_b(Z_0 + Z_c))^2 + (2X_b(Z_0 + Z_c))^2}} \\ \Phi_{12} = tg^{-1}\left(\frac{2Z_cX_b}{2R_bZ_c}\right) - tg^{-1}\left(\frac{2X_b(Z_0 + Z_c)}{((Z_0 + Z_c)^2 + 2R_b(Z_0 + Z_c))}\right) \end{cases} \quad (24)$$

The simulation results of the capacitive RF MEMS switch at the two states OFF (the bridge at downstate) and ON (bridge position $g = 3 \mu\text{m}$) are shown, respectively, in **Figures 7** and **8**.

To validate our model, we simulated the capacitive RF MEMS switch with HFSS. The results are compared in terms of return loss, insertion loss, and phase at the two states of the capacitive RF MEMS switch (ON and OFF). Here, we intend to show the similarity between the results of our model and the software HFSS simulation.

5. RF MEMS-based reconfigurable component design

This section will present the use of RF MEMS switches to obtain different tunable RF devices, namely, a phase shifter, a resonator, and a tunable antenna.

5.1. Reconfigurable phase shifter at 18 GHz based on RF MEMS

The reflection-type phase shifter as shown in **Figure 9** is constituted with hybrid coupler and RF MEMS capacitive switches (i.e., metal-dielectric-metal) [20]. The first RF MEMS is connected between a through-port and ground. The second is linked between the coupled port and ground.

In this design, the tunability is achieved by the use of a capacitive RF MEMS switch acting as a reflection load. The capacitor value, which is controlled by a DC voltage, operates from downstate to upstate. This variable capacitance is used to tune the variable phase shifter.

The reflection-type phase shifter using switch RF MEMS capacitive was implemented in ADS simulation software. The reflection coefficient Γ is given by Eq. (25), where ($X_b = L_b\omega - (1/c_b\omega)$).

$$\Gamma = |\Gamma|e^{j\phi_{21}} = \frac{Z_s - Z_0}{Z_s + Z_0} = \frac{[Z_c^2 + 2Z_cR_b - Z_cZ_0 - Z_0R_b] + jX_b[2Z_c - Z_0]}{[Z_c^2 + 2Z_cR_b + Z_cZ_0 + Z_0R_b] + jX_b[2Z_c + Z_0]} \quad (25)$$

Figure 10 shows the RF phase shifter performance around 18 GHz, in terms of the return and insertion loss, and the phase shift dependency on the applied voltage. Despite not fully linear, it is possible to observe an almost linear characteristic of the phase shifter in different frequency ranges.

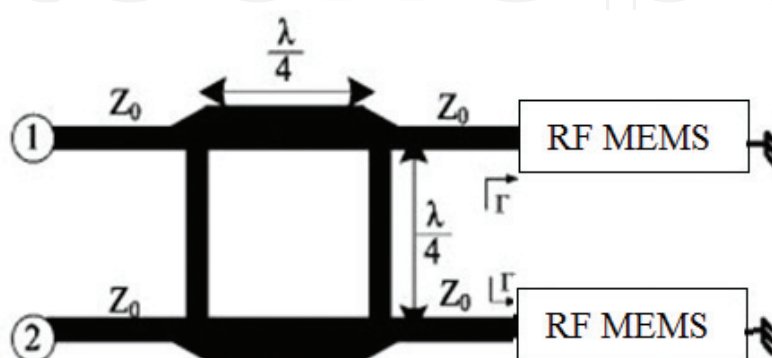


Figure 9. Simulation results of the scattering parameters versus frequency at ON state.

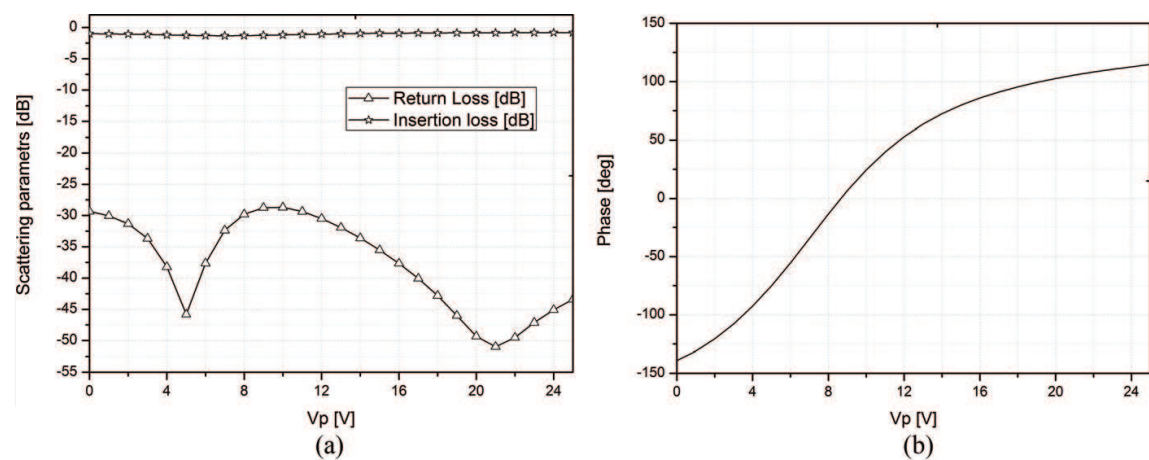


Figure 10. Simulation results of the phase shifter versus the applied voltage at 18 GHz: (a) scattering parameters and (b) phase.

5.2. MEMS-based reconfigurable resonator

There is an important claim that reconfigurable radio-frequency components on a single chip with high performances and multiband characteristics may be a solution for wireless communication [21, 22]. In this study, an improvement of the capacitive RF MEMS structure is proposed in order to obtain a reconfigurable resonator. **Figure 11** shows the suggested RF MEMS resonator structure [23].

The tunable RF MEMS characteristic was designed based on capacitive and inductive effects. The capacitive effect is due to the space between the bridge and the RF line, while the inductive

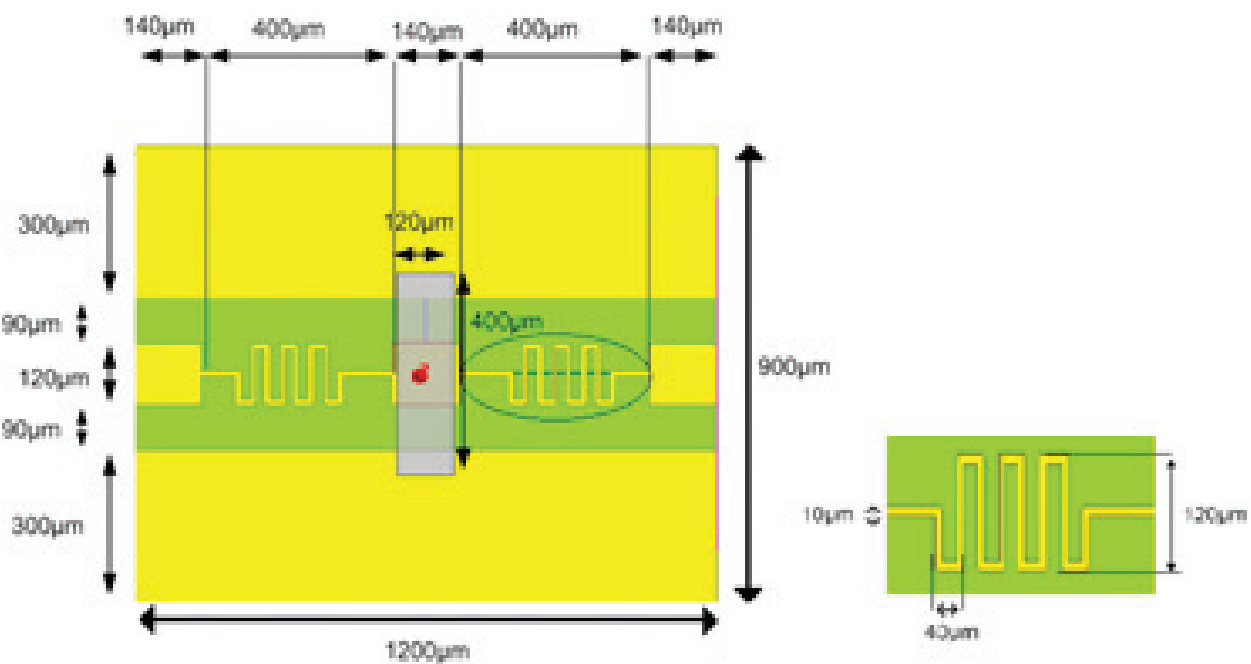


Figure 11. Proposed resonator RF MEMS.

effect is due to the presence of two meander inductors which are integrated in line with the RF waveguide. The combination of these two effects leads to a resonant phenomenon, introducing different resonant frequencies. If the applied voltage V_p is equal to 0 V, the bridge is in the UP state; therefore, the device is at a normally ON state. Moreover, the spacing g between the membrane bridge and the RF line affects the resonance frequency. The spacing g among bridge and CPW line varies between $g = 2\text{ }\mu\text{m}$ at OFF state and $g = 3\text{ }\mu\text{m}$ at ON state.

The proposed tunable resonator was simulated with HFSS and CST-MWS tools. **Figure 12** presents the scattering parameters for different bridge positions, in order to achieve a tunability on the frequency band between 10 GHz and 40 GHz.

Figure 12a and **b** shows, respectively, the return loss (S_{11}) and the insertion loss (S_{12}) for $g = 2, 2.5$, and $3\text{ }\mu\text{m}$. It is possible to observe that controlling the bridge position level allows to obtain three resonant frequencies: 21.9, 24, and 25.1 GHz.

The S_{12} parameter presents almost constant value equal to -1 dB for all simulated spacing g factor when the S_{11} parameter is down to -10 dB . There is a good correspondence between the simulation results on HFSS and CST-MWS simulators.

Table 4 summarizes the spacing g factor versus the applied voltage. Moreover, the resonance frequency and the frequency range in different states of the bridge are shown. The RF MEMS is

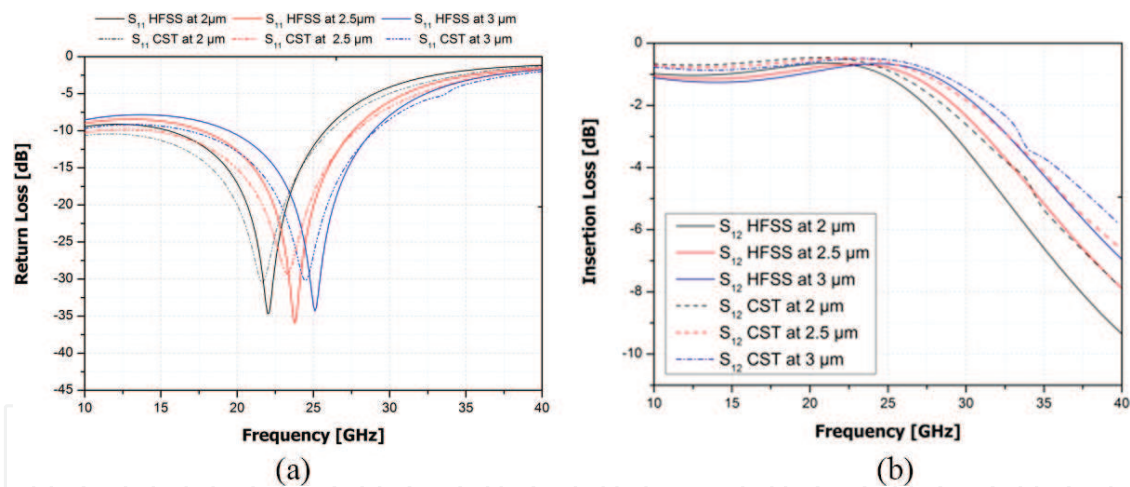


Figure 12. Scattering parameters at $g = 2, 2.5$, and $3\text{ }\mu\text{m}$: (a) return loss (b) insertion loss.

Space $g\text{ (}\mu\text{m)}$	Applied voltage (V)	Cover band			
		Resonance frequency (GHz)		Frequency range (GHz)	
		HFSS	CST	HFSS	CST
2	25 V	21.9	21	15.6–25.7	10–26.1
2.5	19 V	24	23.1	17.8–27.6	14.4–27.8
3	0 V	25.1	24.6	19.5–29	16.8–29

Table 4. Simulation results of the proposed resonator.

normally ON component, i.e., at $g = 3\text{ }\mu\text{m}$, the applied voltage equal to 0 V. This table presents a comparison study of the simulation results of the resonator between HFSS and CST-MWS. The proposed resonator covers three bands.

5.3. Reconfigurable antenna based on a RF MEMS resonator

Figure 13 presents the structure of the proposed reconfigurable CPW antenna [24], which is based on the integration of a resonating RF MEMS device with the CPW antenna on the same substrate. The reconfigurability of this antenna depends on the load provided by the state of

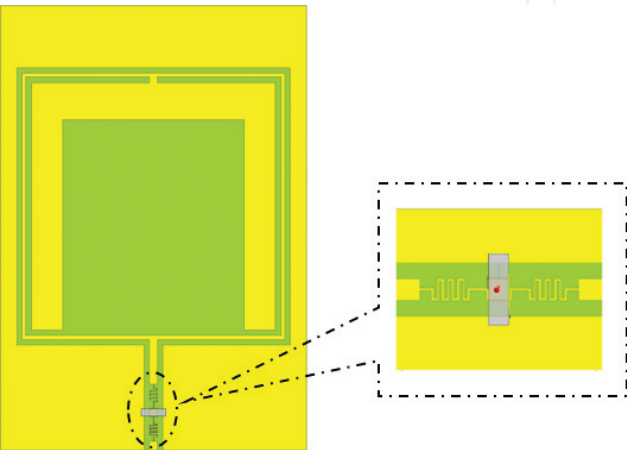


Figure 13. Reconfigurable antenna based on RF MEMS.

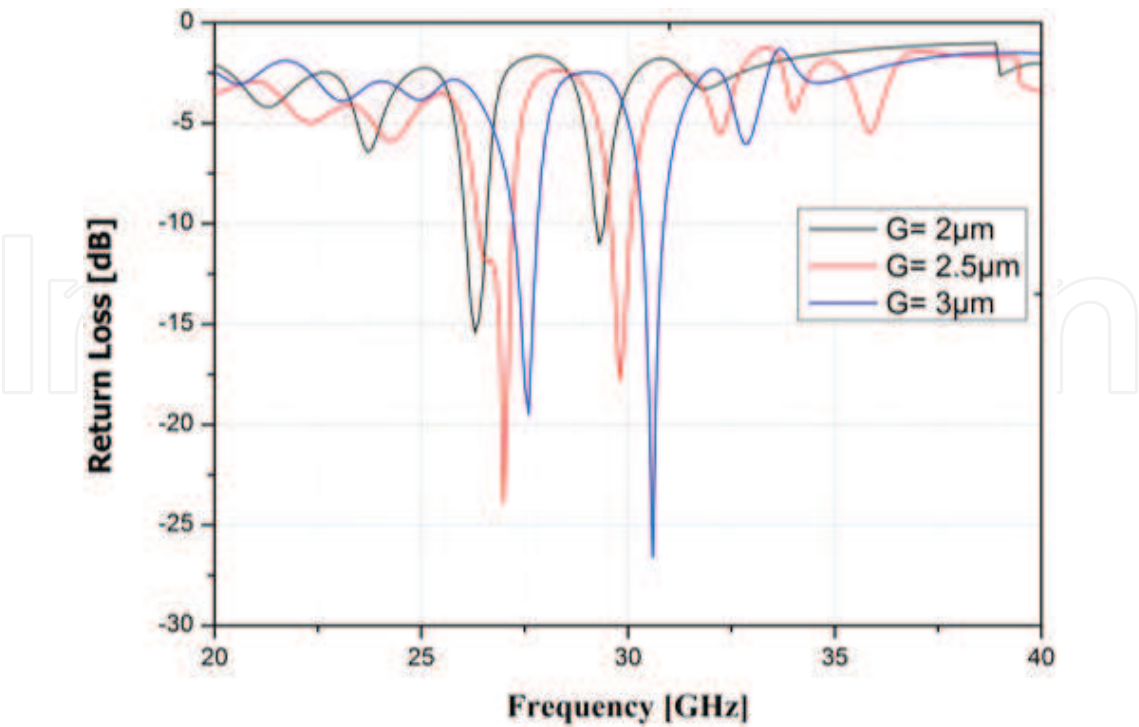


Figure 14. Return loss results versus frequencies.

the RF MEMS resonator. The antenna considered was a modified patch antenna with a printed inverted U-shaped ring resonator.

Figure 14 shows the reflection coefficient simulation results. The resonant frequencies can be observed at three states of the bridge. For $g = 2 \mu\text{m}$, the device has a single resonant frequency of 26.3 GHz, and the return loss will be 15.1 dB; for $g = 2.5 \mu\text{m}$, it shows two resonant frequencies: first at 27 GHz with a return loss of 23 dB and, second at 29.8 GHz with a return loss of 18 dB; and for $g = 3 \mu\text{m}$ with also two resonant frequencies: 27.5 and 30.6 GHz, with return loss of 19.84 dB and 26.62 dB, respectively.

Figure 15 shows the radiation pattern for different resonance frequencies at three different antenna configuration states, considering $\phi = 90^\circ$. Firstly, the three states bridge given three resonance frequencies and the main lobe at $\theta = 310^\circ$. Secondly, only for $g = 2.5$ and $g = 3 \mu\text{m}$ given the resonance frequency and the main lobe at $\theta = 0^\circ$.

Table 5 summarizes the simulation results of the reconfigurable antenna in terms of the spacing g factor versus the applied voltage, the resonant frequencies, the return loss, bandwidths, and gains.

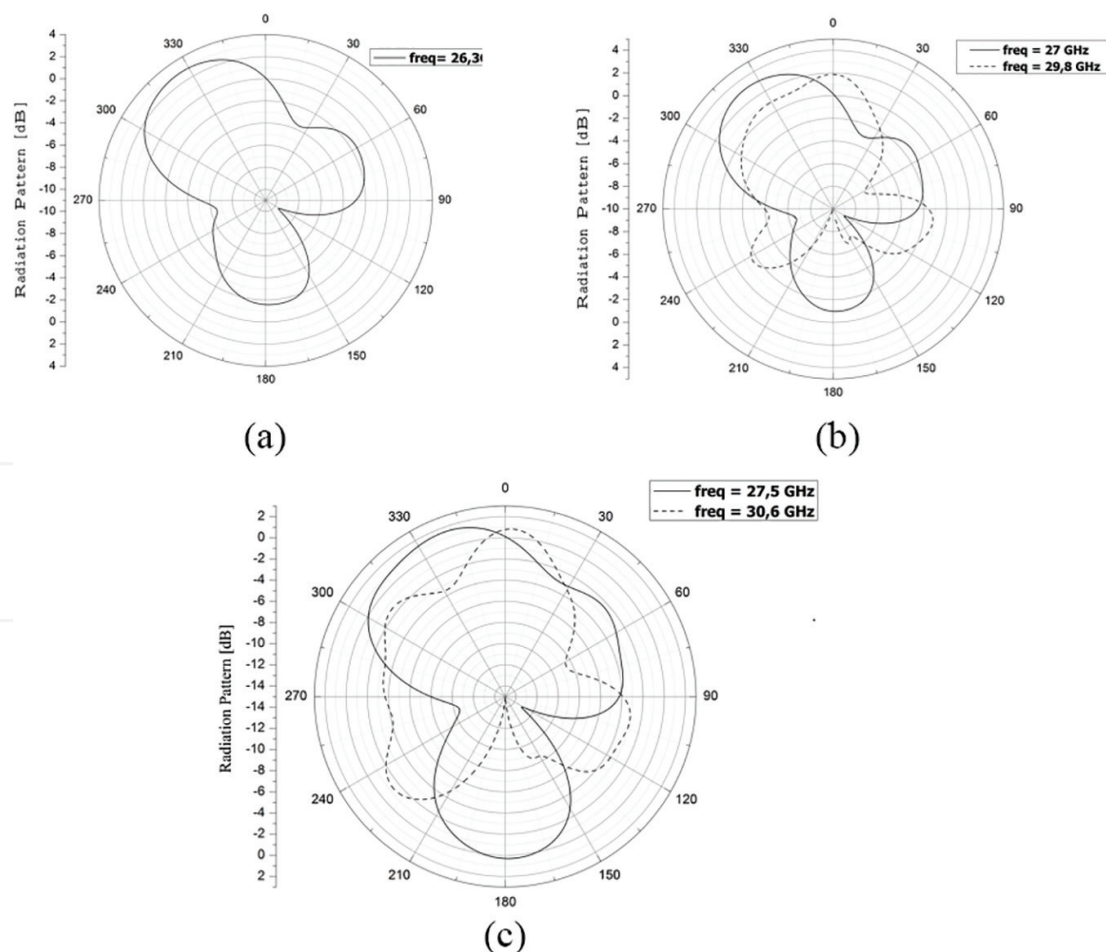


Figure 15. Realized gain of the reconfigurable antenna at different states: (a) at $2 \mu\text{m}$, (b) at $2.5 \mu\text{m}$, and (c) at $3 \mu\text{m}$.

Parameters	Values				
Space g (μm)	2	2.5		3	
Applied voltage (V)	25	19		0	
Resonance frequency (GHz)	26.3	27	29.8	27.5	30.6
RL (dB)	15.1	23	18	18.84	26.62
Frequency range (GHz)	26–26.6	26.4–27.3	29–30.1	27.3–28	30.13–30.7
BW (%)	2.281	3.333	3.691	2.545	1.863
Gain (dB)	3	3	2	2	1

Table 5. The reconfigurable antenna results.

6. Conclusions

In this chapter, we have developed a parametric model for a capacitive RF MEMS switch in the frequency range between 1 and 40 GHz. A comparative study was carried out to analyze the theoretical model's mechanical characteristic with COMSOL and to compare the theoretical electrical properties (return loss, insertion loss, and phase) to those obtained using HFSS. The proposed model computes the input data swiftly and efficiently and produces results similar to those obtained with the aforementioned simulation software, while being much faster and less resource-demanding.

It was also presented the design, the analysis, and the simulation of the reflection-type phase shifter, using integrated RF MEMS switches. The proposed phase shifter at 18 GHz, which has approximately a constant insertion loss (≈ -1 dB) with a significant return loss (< -30 dB) and phase shift (-138.822° and 128.15°), can be used in different RF applications, namely, it is suitable for radar applications.

We have analyzed a new contribution for RF MEMS to obtain a tunable resonator. The idea of this reconfigurable resonator is based on the use of two meander inductors and a variable capacitance. The simulation of this component was made by two electromagnetic design tools, and there was good agreement between them for different tuning conditions (spacing states of $g = 2, 2.5$ and $3 \mu\text{m}$). The obtained resonance frequencies for the three considered states were, respectively, 21.9, 24, and 25.1 GHz. The bandwidths were [15.6, 25.7], [17.8, 27.6], and [19.5, 29] GHz, respectively, demonstrated for the three resonant frequencies ($|S_{11}| = 35$ dB and $|S_{12}| = 1$ dB). This resonator switches can be used in different RF applications, for example, at K and Ka bands.

We have also proposed a reconfigurable antenna based on the association between the last resonator and the CPW antenna to obtain tunability at Ka band. For $g = 2 \mu\text{m}$, a single resonant frequency of 26.3 GHz was obtained, with a return loss of 15.1 dB and a realized gain equal to 3 dB; for $g = 2.5 \mu\text{m}$, two resonant frequencies of 27 and 29.8 GHz were obtained, with a return loss of 23 and 18 dB and a realized gain 3 and 2 dB. Finally, for $g = 3 \mu\text{m}$, it also allows two resonant frequencies, 27.5 and 30.6 GHz, with a return loss of 19.84 and 26.62 dB, showing a realized gain of 2 and 1 dB, respectively.

Acknowledgements

This work was supported by the Laboratory of Circuit and Electronic System in High Frequency of University of Tunis El Manar and Research Center for Microelectromechanical Systems (CMEMS) of the University of Minho Braga-Portugal. Foundation for Science and Technology (FCT) project PTDC/EEI-TEL/5250/2014, by FEDER funds through POCI-01-145-FEDER-16695 and Projecto 3599-Promover a Produção Científica e Desenvolvimento Tecnológico e a Constituição de Redes Temáticas.

Author details

Bassem Jmai^{1*}, Adnen Rajhi^{2,3}, Paulo Mendes⁴ and Ali Gharsallah¹

*Address all correspondence to: bassem.jmaiesti@gmail.com

1 Department of Physics, FST, Unit of Research in High Frequency Electronic Circuit and System, University Tunis El Manar, Tunis, Tunisia

2 Department Electrical Engineering, National School of Engineering Carthage, Tunis, Tunisia

3 Laboratory of Physics Soft Materials and EM Modelisation, FST, University Tunis El Manar, Tunis, Tunisia

4 Department of Industrial Electronics, Microelectromechanical Systems Research Center, University of Minho, Guimarães, Portugal

References

- [1] Gevorgian S. *Ferroelectrics in Microwave Devices, Circuits and Systems: Physics, Modeling, Fabrication and Measurements*. Springer Science & Business Media; 2009. ISBN: 9781848825062
- [2] Sharma M, Kuanr BK, Sharma M, Basu A. Tunable coplanar waveguide microwave devices on ferromagnetic nanowires. *International Journal of Materials, Mechanics and Manufacturing*. February 2014;**2**(1):9-13. DOI: 10.7763/IJMMM.2014.V2.88
- [3] El Cafsi MA, Nedil M, Osman L, Gharsallah A. The design of a 360°-switched-beam-base station antenna. In: *Antenna Arrays and Beam-formation*. Rijeka: InTech; May 2017. pp. 13-30. ISBN: 978-953-51-3146-5
- [4] Mabrouki M, Jmai B, Ghyoula R, Gharsallah A. Miniaturisation of a 2-bits reflection phase shifter for phased array antenna based on experimental realisation. *International Journal of Advanced Computer Science and Applications*. May 2017;**8**(5):438-454. DOI: 10.14569/IJACSA.2017.080553
- [5] Rijks TG, Steeneken PG, Beek JTM, Ulenaers MJE, Jourdain A, Tilmans HAC, Coster JD, Puers R. Microelectromechanical tunable capacitors for reconfigurable RF architectures.

- Journal of Micromechanics and Microengineering. February 2006;**16**(3):601-611. DOI: 10.1088/0960-1317/16/3/016
- [6] De Los Santos Héctor J. RF MEMS Circuit Design for Wireless Communications. Artech House; 2002. ISBN: 1-58053-329-9
 - [7] Brown ER. RF-MEMS switches for reconfigurable integrated circuits. IEEE Transactions on Microwave Theory and Techniques. November 1998;**46**(11):1868-1880. DOI: 10.1109/22.734501
 - [8] Rebeiz GM. RF MEMS, Theory, Design and Technology. John Wiley & Sons; 2003. ISBN: 978-0-471-20169-4
 - [9] Dussopt L, Rebeiz GM. High-Q millimeter-wave MEMS varactors: Extended tuning range and discrete-position design. IEEE MTT-S International Microwave Symposium Digest. June 2002;**2**:1205-1208. DOI: 10.1109/MWSYM.2002.1011869
 - [10] Blondy P, Mercier D, Cros D, Guillon P, Rey P, Charvet P, Diem B, Zanchi C, Lappierre L, Sombrin J. Packaged millimeter wave thermal MEMS switches. In: IEEE 31st European Microwave Conference; 24–26 September 2001
 - [11] Park JY, Yee YJ, Nam HJ, Bu JU. Micromachined RF MEMS tunable capacitors using piezoelectric actuators. In: IEEE International MTT-S Microwave Symposium Digest; 20–24 May 2001
 - [12] Ruan M, Shen J, Wheeler CB. Latching micromagnetic relays. IEEE Journal of Microelectromechanical System. December 2001;**10**:511-517. DOI: 10.1109/84.967373
 - [13] Mafinejad Y, Kouzani A, Mafinezhad K. Review of low actuation voltage RF MEMS electrostatic switches based on metallic and carbon alloys. Journal of Microelectronics, Electronic Components and Materials. May 2013;**43**(2):85-96
 - [14] Muller Ph. Conception, Fabrication et Caractérisation d'un Microcommutateur Radio Fréquences pour des Applications de Puissance [PhD thesis]. L'université des sciences et technologies de Lille UFR d'électronique, Lille 1; 2005
 - [15] Lonac JA, Merletti GA. Parametric analysis on the design of RF MEMS series switches. European Scientific Journal. December 2015;**1**:248-257. ISSN: 1857-7431
 - [16] Brown ER. RF-MEMS switches for reconfigurable integrated circuits. IEEE Transactions on Microwave Theory and Techniques. November 1998;**46**(11):1868-1880. DOI: 10.1109/22.734501
 - [17] Caekenberghe KV. Modeling RF MEMS devices. IEEE Microwave Magazine. January 2012;**13**(1):83-110. DOI: 10.1109/MMM.2011.2173984
 - [18] Jmai B, Rajhi A, Gharsallah A. Controllable bridge of the RF-MEMS: Static analysis. In: International Conference on Green Energy Conversion Systems (GECS); October 2017
 - [19] Jmai B, Anacleto P, Mendes P, Gharsallah A. Modeling, design, and simulation of a radio frequency microelectromechanical system capacitive shunt switch. International Journal

Numerical Modeling, Electronic Networks, Devices and Fields. 2017:e2266. DOI: 10.1002/jnm.2266

- [20] Jmai B, Rajhi A, Gharsallah A. Conception of a tunable analog reflection-type phase shifter based on capacitive RF MEMS for radar application. *International Journal of Microwave and Optical Technology*. September 2016;**11**(5):339-346. DOI: IJMOT-2016-6-1031
- [21] Chun YH, Hong JS. Electronically reconfigurable dual-mode microstrip open-loop resonator filter. *IEEE Microwave and Wireless Components Letters*. July 2008;**18**(7):449-451. DOI: 10.1109/LMWC.2008.924922
- [22] Rinaldi M, Zuo C, Vander Spiegel J, Piazza G. Reconfigurable CMOS oscillator based on multifrequency AlN contour-mode MEMS resonators. *IEEE Transactions on Electron Devices*. May 2011;**58**(5):1281-1286. DOI: 10.1109/TED.2011.2104961
- [23] Jmai B, Rajhi A, Gharsallah A. Novel conception of a tunable RF MEMS resonator. *International Journal of Advanced Computer Science and Applications*. January 2017;**8**(1):73-77. DOI: 10.14569/IJACSA.2017.080111
- [24] Jmai B, Gahgouh S, Gharsallah A. A novel reconfigurable MMIC antenna with RF-MEMS resonator for radar application at K and Ka bands. *International Journal of Advanced Computer Science and Applications*. May 2017;**8**(5):468-473. DOI: 10.14569/IJACSA.2017.080556

IntechOpen

